Sub-micron Cu/SSZ-13: synthesis and application as selective catalytic reduction (SCR) catalysts

Sebastian Prodinger,[a] Miroslaw A. Derewinski,[a,*] Yilin Wang,[a] Nancy M. Washton,[b] Eric D. Walter,[b] János Szanyi,[a] Feng Gao,[a,*] Yong Wang,[a,c] and Charles H. F. Peden[a]

[a)] Institute for Integrated Catalysis, Pacific Northwest National Laboratory, P.O. Box 999, Richland, WA 99352, United States

[b)] Environmental Molecular Sciences Laboratory, Pacific Northwest National Laboratory, P.O. Box 999, Richland, WA 99352, United States

[c)] School of Chemical and Biological Engineering, Washington State University, Pullman, WA 99364, United States

KEYWORDS. selective catalytic reduction, Cu/SSZ-13, zeolite synthesis, particle size, hydrothermal aging.

ABSTRACT: For the first time, sub-micron Cu/SSZ-13, obtained by modifying an existing synthesis procedure, was shown to be an effective and stable catalyst for selective catalytic reduction of NO. Characterization of the materials with X-ray diffraction, N_2-physisorption and ^{27}Al MAS NMR shows that hydrothermal aging, which simulates SCR reaction conditions, is more destructive for smaller particles in a sodium form. After Cu exchange, however, the catalytic performance and hydrothermal stability for Cu/SSZ-13 is independent of the particle size. In particular, a clear positive correlation is found between remaining tetrahedral framework Al and isolated Cu-ion concentrations in aged Cu/SSZ-13 catalysts of comparable Al and Cu contents. This indicates that (1) isolated Cu-ion and paired framework Al configurations display remarkable hydrothermal stabilities; and (2) paired-Al contents can be varied via modifying the synthesis procedures, which appear to have a more critical influence on stabilizing isolated Cu-ions during harsh hydrothermal aging than the particle size. This study is of high interest for applications in vehicular DeNOx technologies where high loadings of active species on wash coats can be achieved by using sub-micron Cu/SSZ-13.

1 INTRODUCTION

© 2016. This manuscript version is made available under the Elsevier user license
http://www.elsevier.com/open-access/userlicense/1.0/

Copper-ion exchanged SSZ-13 has been successfully commercialized as a diesel engine exhaust after-treatment catalyst since 2010 [1, 2]. The current generation Cu/SSZ-13, for example the catalyst provided by BASF Corporation used on light duty diesel vehicles in the USA, has a Si/Al ratio of ~17.5 and Cu loading of ~2.8 wt%, corresponding to a 100% ion exchange level (exchange level = $\frac{mol(Cu)}{mol(Al)} \times 200\%$) [3]. This catalyst is optimized to operate in the temperature window between ~200 and ~400 °C. At higher operation temperatures, this catalyst loses SCR efficiency because of the competitive, non-selectivity NH_3 oxidation reaction. There have been continuous efforts aiming at improving the performance (activity, selectivity and stability) of the current generation catalysts. Towards this goal, an atomic level understanding of the nature of the active sites is crucial.

Over the past few years, it has become generally accepted that Cu/SSZ-13 contains two primary Cu coordination geometries: Cu^{2+} ions that are associated with two framework Al sites (Al pairs), and $[Cu(OH)]^+$ ions that are associated with one framework Al. Both experimental and theoretical studies demonstrate that the former species interact more strongly with the zeolite framework [4-10]. Recently, Paolucci et al. have shown that in SSZ-13 with a random framework Al distribution, the latter populate upon saturation of the former species [10]. Assertions have been made that the former species are active for SCR, while the latter and other minority species (e.g., oligomeric CuOx species) catalyze non-selective side reactions [11, 12]. Our recent study has revealed, however, that Cu/SSZ-13 catalysts with high Si/Al ratios (e.g., 35) do catalyze low-temperature SCR efficiently [8]. Note that in such catalysts, the possibility for Cu^{2+} ions to interact with framework Al pairs is small and $[Cu(OH)]^+$ ions that interact with single Al site dominate. Therefore, this study demonstrated that both Cu^{2+} and $[Cu(OH)]^+$ ions in Cu/SSZ-13 are SCR active. Interestingly, the recent theoretical work by Paolucci et al. [10] indeed demonstrated rather similar activation and reaction energies for the two active sites. Note, however, weaker interactions between $[Cu(OH)]^+$ ions and the SSZ-13 framework make these species hydrothermally less stable, which tend to agglomerate to form undesirable CuOx clusters during aging. Therefore,

it is anticipated that only Cu^{2+} ions associated with paired framework Al sites maintain excellent stability and SCR selectivity in hydrothermally aged catalysts. This understanding provides some general guidelines for the synthesis of Cu/SSZ-13 catalysts for use: (1) for low-temperature activity enhancement, catalysts with high exchange levels appear appropriate; (2) to maintain good SCR selectivities after hydrothermal aging, catalysts with low to intermediate exchange levels, where the majority of Cu^{2+} ions are associated with paired framework Al sites, appear appropriate. However, a low Cu-loaded catalyst may not possess the required hydrothermal stabilities. Recently, it has been shown that by introducing alkali and alkaline earth co-cations to low Cu-loaded Cu/SSZ-13, both low-temperature activity and hydrothermal stability can be enhanced [13]. In this case, the introduction of co-cations weakens Cu-zeolite interactions thus lowering redox barriers of Cu-ions; meanwhile, the neutralization of some Brønsted acid sites enhances hydrothermal stability of the catalysts.

Besides the above-mentioned parameters, i.e., Si/Al ratio [8], Cu loading [6, 7], and Brønsted acid site densities [8] that are manipulated in order to synthesize better catalysts, morphology and particle size of the SSZ-13 material may also impart effects on the performance and stability of Cu/SSZ-13 catalysts. These broadly defined geometric effects, to our knowledge, have not been investigated to date. In this contribution, a few readily reproducible SSZ-13 synthesis methods, which allow for the generation of SSZ-13 with different morphology and particle sizes, are described. These SSZ-13 materials are then used in the synthesis of Cu/SSZ-13 catalysts, where their SCR performance and hydrothermal stability are investigated.

2 EXPERIMENTAL PROCEDURE

2.1 SSZ-13 synthesis

Method A: This method has been reported recently by Gao et al. [8], which, in turn, was adapted from a recipe provided by Deka et al. [14]. In short, the composition of the gel was as follows: 10TMAda-

OH:5Na_2O:4Al_2O_3:100SiO_2:2200H_2O. Preparation of the gel involved first dissolving NaOH in water followed by addition of the structure directing agent TMAda-OH (Sachem Zeogen 2825, 24.8wt% in H_2O). In the next step, aluminum hydroxide (containing ~54% Al_2O_3, Aldrich) was added slowly, and the stirred solution was kept at room temperature until it became clear. Slow addition of fumed silica (0.007 μm average particle size, Aldrich) under vigorous stirring, followed by aging for two hours, then yielded a homogeneous gel. This mixture was then placed in an autoclave fitted with a Teflon liner and Teflon-coated magnetic stir bar and heated to 160°C on a stir plate. Hydrothermal synthesis was carried out at this temperature and stirring conditions (300 rpm) for 96 h. It should be noted that stirring is essential for a homogeneously crystallized material [8]. Upon completion, the crystalline material was separated from the mother solution via centrifugation and washed several times until a close to neutral pH could be measured. The zeolite powder was then dried in an oven at 100°C overnight.

Method B: This novel procedure[15], allowing synthesis of sub-micron SSZ-13, is an adaption of *Method A*. In essence the gel composition and aging time was changed. The gel composition was as follows: 20TMAda-OH:10Na_2O:4Al_2O_3:100SiO_2:4400H_2O. First, NaOH was dissolved in H_2O followed by sequential addition of $Al(OH)_3$ and TMAda-OH. The solution was kept under stirring conditions at room temperature until it became clear, followed by the slow addition of fumed silica. The gel was then aged for 24 h before being placed in a Teflon lined autoclave in a rotating oven at 160°C for 96 h. Sample separation, wash and dry procedures were the same as in procedure A.

Method C: The same gel composition and preparation described in method B was used. The aged gel underwent hydrothermal synthesis in a Teflon lined autoclave at 160 °C under stirring (300rpm) for 96 h on a stir plate. The following procedures consisting of separation, washing and drying were the same as for methods A and B.

The as-made materials obtained with methods A, B and C were then placed in a tube furnace and heated to 550 °C in flowing air at 1 °C/min, and maintained for 8 h to fully decompose the template to

obtain Na/SSZ-13 A, B or C. Based on ICP and TGA analyses shown below, Na^+/H^+ ratios in these samples are ~0.66.

2.2 Cu/SSZ-13 synthesis

The ion exchange procedure to synthesize Cu/SSZ-13 was as follows: 2 g of Na/SSZ-13 A, B or C and 100 ml 0.01M $CuSO_4$ solution were mixed and a few drops of 1.0 M HNO_3 solution were added to adjust the pH to ~3.0. Under stirring (300 rpm), the mixture was heated to 80 °C, and maintained for 1 h. After the exchange, solid Cu/SSZ-13 was collected via centrifugation, washed with deionized water for three times, and dried in flowing air at 120 °C. Following which, it was calcined in static air at 550 °C for 5 h. Catalysts thus generated are defined as fresh catalysts, and are abbreviated as Cu/SSZ-13 A, B or C here, where A, B and C represent the corresponding SSZ-13 synthesis methods described above. A portion of the fresh catalysts were hydrothermally aged in flowing air containing 10% water vapor at 800 °C for 16 h. Catalysts thus treated are defined as HTA catalysts, abbreviated as Cu/SSZ-13_{HTA} A, B or C.

To study hydrothermal stability for samples in the Na form, fresh Na/SSZ-13 samples also underwent hydrothermal aging in flowing air containing 10% water vapor at 700 °C for 3h. These samples are denoted Na/SSZ-13_{HTA*} A, B or C.

2.3 Catalyst Characterization

X–ray diffraction (XRD) patterns were collected on a Rigaku Mini Flex II bench top X–ray diffractometer using a Cu–Kα radiation of 0.154056 nm (30 kV and 15 mA). Experiments were conducted on a powder sample holder in a 2θ range of 5 to 60°, with a step size of 0.02 °/s. All measurements were performed under ambient conditions.

X'pert Highscore Plus software was used for a deconvolution of the diffraction data using a Voigt function. The sample displacement was set at 0.1 mm and the zero shift at 0.00025. Both values were

determined through refinement and kept constant for the deconvolution process. The obtained FWMH values along with a shape factor of 0.9 were then used to calculate the crystallite size using the Scherrer equation. Average crystallite sizes are reported in the Supporting Information (Table S1).

Helium ion microscopy (HIM) images were obtained using 35 keV He ions with 0.1 pA beam current at normal incidence. Secondary electrons were detected using an Everhart–Thornley detector. For HIM imaging, a very thin layer of carbon (<1 nm) was coated using a carbon sputter deposition system as the samples were completely insulating. The instrument resolution was 0.35 nm. A particle size distribution was obtained by visually measuring and analyzing 100 particles seen in the helium ion micrographs.

N_2-physisorption information for pore volumes was obtained using a Micromeritics ASAP 2020 setup. A DFT method optimized for N_2 on oxide surfaces, provided by the Micromeritics software suite, was applied to assess the micropore volume contributions. Single point adsorption close to $p/p_0 = 0.99$ was used to determine the total pore volume.

Thermogravimetric and calorimetric (TGA-DSC) analysis was conducted on a Netzsch STA 449C Jupiter system to investigate template removal of the as-synthesized materials. Fresh, dried samples were heated up to 1000 °C at a rate of 5 °C/min under a flow of N_2 and N_2/O_2.

Elemental Analysis was performed using two methods: Cu and Na contents of the fresh Cu/SSZ-13 samples were determined with Inductively Coupled Plasma Atomic Emission Spectroscopy (ICP-AES) at Galbraith Laboratories (Knoxville, TN, USA). A more detailed elemental analysis on the C series of samples was performed in house with Atomic Absorption Spectroscopy (AAS). A Unicarn M Series Flame-Atomic Absorption spectrometer equipped with an FS95 autosampler and a GF95 graphite furnace was used to determine the elemental composition of the samples.

^{27}Al MAS NMR direct polarization experiments were conducted on a 20 Tesla wide bore Varian VNMRs spectrometer, utilizing a 1.6 mm triple resonance probe operating in HX mode tuned to an ^{27}Al frequency of 221.4119 MHz. Spectra were acquired by collecting 14336 transients using calibrated ^{27}Al

π/20 pulses of 0.25 us, a 1250 kHz sweep width, a spinning speed of 34 kHz, and a 0.5 s recycle delay. Time domain free induction decays were apodized with exponential functions corresponding to 200 Hz of Lorentzian broadening prior to Fourier transformation. ^{27}Al resonances were referenced to 0.1 M $AlCl_3$(aq) at 0 ppm. To ensure full hydration of the samples, they were placed in a desiccator over saturated $Ca(NO_3)_3$ solution for a minimum of 48h. The different Al species were assessed by deconvoluting the spectra with Lorentzian/Gaussian peak shapes, using the same line shape for each respective peak (tetrahedral, pentahedral and octahedral) across all samples and allowing the remaining parameters to be optimized. An example of a typically fitted spectrum is shown in the supporting information (Figure S8). To determine the Al content quantitatively, a reference SSZ-13 zeolite of comparable known Al content was used as external reference [15].

Electron paramagnetic resonance (EPR) experiments were conducted on a Bruker E580 X-band spectrometer equipped with a SHQE resonator and a continuous flow cryostat [16]. Powder samples (~10 mg) were contained in 4 mm OD quartz tubes. Microwave power was 20 milliwatts, and the frequency was 9.34 GHz. The field was swept by 6000 G in 84 s and modulated at 100 kHz with 10 G amplitude. A time constant of 41 ms was used. Quantification of isolated Cu^{2+} ions was done by using standard solutions of Cu(II)-imidazole.

NH_3 Temperature programmed desorption (TPD) was conducted on samples (0.1g) that were first activated under flowing O_2/N_2 at 550 °C for 30 min. They were then saturated with 1% NH_3/He at 160 °C, and purged with 300 sccm N_2 for 3h at 160 °C to remove weakly adsorbed species. Subsequently, NH_3-TPD was conducted by ramping the sample temperature at 10 °C /min until NH_3 desorption was complete. NH_3 desorption was monitored with a FTIR gas analyzer (MKS 2030).

2.4 Standard NH_3-SCR reaction tests

NH_3-SCR reaction kinetics measurements were carried out in a plug-flow reaction system described elsewhere [11]. Powder samples were pressed, crushed and sieved (60-80 mesh) prior to use. For stan-

dard SCR, the feed gas contained 350 ppm NO, 350 ppm NH_3, 14% O_2, 2.5% H_2O and balance N_2. All of the gas lines were heated to over 100 ºC to avoid water condensation. The total gas flow was 300 sccm, and the gas hourly space velocity (GHSV) was estimated to be ~200,000 h^{-1}. Concentrations of reactants and products were measured by an online Nicolet Magna 560 FTIR spectrometer with a 2 m gas cell maintained at 150 ºC.

3 RESULTS AND DISCUSSION

3.1 Synthesis of SSZ-13 with different particle sizes

XRD patterns for the as-made and calcined Na/SSZ-13 samples (Figure S1) demonstrate that these are highly crystalline, with all reflections matching the CHA framework type [17]; no amorphous or other crystalline phases were detected.

Table 1. Sorption properties of materials synthesized with different procedures.

Sample	Micropore volume [cm^3/g]	Mesopore volume [cm^3/g]	Total pore volume* [cm^3/g]
Na/SSZ-13 A	0.29	0.02	0.31
Na/SSZ-13 B	0.29	0.06	0.35
Na/SSZ-13 C	0.27	0.22	0.49

*Total pore volume determined with single point adsorption close to p/p_0 0.99.

Table 1 displays pore volumes of the calcined Na/SSZ-13 samples. All synthesis methods led to materials with almost identical micropore volume. Note, however, larger contribution of mesopores is found for materials synthesized using methods B and C, especially method C. The type of mesopores can be

identified by the hysteresis at p/p_0 >0.7, which is typically associated with inter-crystalline mesopores (Figure S3) [18]. This type of mesoporosity is due to a large degree of agglomeration, which can also be seen with helium ion microscopy (HIM) [19, 20]. The helium ion micrographs in Figure 1 clearly show different particle sizes and morphologies based on the synthesis method chosen. Particle size distribution by measuring the diameters of particles seen in HIM images can be found in the supporting information (Figure S5). Using method A, well-separated particles with some intergrowth and a mean particle diameter measuring 1.3 μm are formed. These primary particles tend to aggregate into larger clusters measuring up to 5 μm. Applying the modified methods B and C, much smaller primary particles, with average particle sizes of 450 and 260 nm, respectively, are generated. These results indicate much higher nucleation rates during synthesis in methods B and C as compared to method A. Crystal growth in zeolites takes place in several phases [21-24]. Initially, the silica source has to be depolymerized in the gel during the aging period. Mineralizing agents such as hydroxyl ions catalyze the depolymerization step [24]. Amorphous aluminosilicates are thus formed, leading to a supersaturated solution upon heating. The nucleation rate is virtually zero until a critical value of supersaturation is achieved and crystal growth is facilitated. The modified methods B and C had extended aging periods compared to method A. By increasing the aging time significantly, more amorphous alumina-silica species are formed, eventually yielding smaller crystallites. Additionally, the Na/Al gel ratio was doubled in methods B and C, which also contributed to more depolymerized silica. Furthermore, XRD data of the Na/SSZ-13 samples (Figure S1) were used to determine crystallite size; the results followed the same trend as observed by microscopy (Supporting Information Table S1). However, some discrepancy between crystallite size derived from XRD and particle size derived from imaging was found. This can be attributed to the limitations of the Scherrer equation and the inherent difference between using grain analysis (microscopy) and coherently scattering domains (XRD) in generating the respective size information [25].

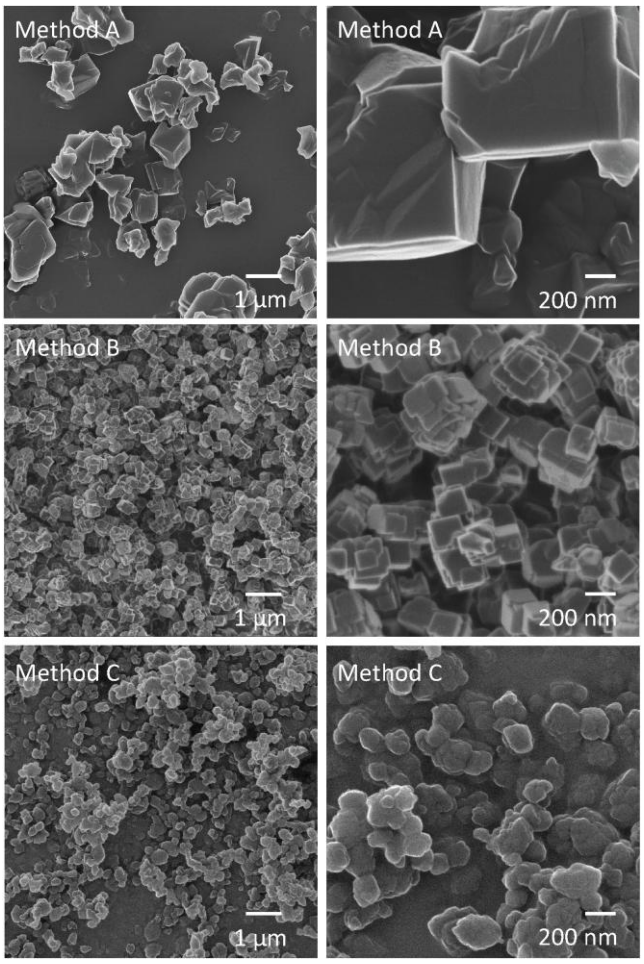

Figure 1. Helium ion micrographs of samples synthesized with methods A-C. The magnifications are listed in the legend.

Interestingly, a clear distinction in the particle morphology due to the choice of agitation can also be seen. Agitation is known to speed up crystal growth rates [26], affect the overall particle size [15] as well as change the framework type [27]. Small round crystals with some intergrowth are formed under stirring conditions (Method C), while small cubic crystals with a moderate degree of intergrowth are formed under rotating conditions (Method B). The stirring speed was significantly faster (300 rpm) than the rotational speed of the autoclaves in the rotating oven (50 rpm). Thus, the degree of homogeneity of supersaturation reached in stirring conditions was higher than in rotating conditions leading to slightly larger particles in the latter. It is worth noting that changes in particle size/shape also affected SDA decomposition as analyzed using a TGA/DSC setup; details are presented in the Supporting Information (Figure S6).

3.2 Selective catalytic reduction (SCR) reaction

The performance of catalysts in SCR reactions depends on several factors such as the Cu loading and the hydrothermal stability. For zeolite catalysts, it is generally found that small particles present a lower hydrothermal stability [28-32]. A possible explanation for this phenomenon is that small particles tend to have more Al present near the surface, facilitating an easier dealumination process without any diffusion limitations [15, 33]. For the present study, our primary aim is to compare catalysts with similar composition, but different particle size/morphology. In order to illustrate this effect and have a fair comparison in SCR performance for the three Cu/SSZ-13 catalysts, it is essential that they have similar Al and Cu contents. By integrating the peak areas in ^{27}Al MAS NMR of the three parent Na/SSZ-13 materials, they indeed have similar amounts of Al incorporated (Table 2). The accuracy of NMR quantification was further confirmed by examining Al content in one of the Na/SSZ-13 samples using elemental analysis. To achieve similar Cu loadings in different samples, a $CuSO_4$ solution that contained Cu^{2+} less than that required for ~50% ion-exchange level was applied in ion exchange. At such Cu^{2+} deficient concentrations, essentially all Cu^{2+} ions in solution are exchanged into SSZ-13. As displayed in Table 2, all three Cu/SSZ-13 catalysts indeed have similar Cu loadings as determined from elemental analysis. Interestingly, even though Na/SSZ-13 samples were used for ion exchange, and Na contents were ~1.5 wt% in all three Na/SSZ-13 samples, in the final products Na levels are very low (< 0.1 wt%). This indicates that under the ion-exchange conditions (i.e., 80 °C and pH ~ 3.0), Cu^{2+} exchanges almost exclusively Na^+ cations. The residual Na does not expect to play a role in affecting catalytic properties of the catalysts. Note also that Al contents in the Cu/SSZ-13 samples are ~7% less than the parent materials due to minor Al loss during ion exchange. Based on the Al and Cu contents in Cu/SSZ-13 samples, Cu/Al ratios are readily calculated; and these are also displayed in Table 2.

Table 2: Al, Cu and Na contents of the fresh Cu/SSZ-13 samples.

Sample	Al [a)] wt%	Cu [b)] wt%	Na [b)] wt%	Cu/Al [c)]
Cu/SSZ-13 A	4.55	1.47	0.046	0.15
Cu/SSZ-13 B	4.50	1.45	0.064	0.15
Cu/SSZ-13 C	4.70	1.62	0.079	0.16

[a)] Al contents of the parent Na/SSZ-13 materials, determined by integration of peaks in ^{27}Al MAS NMR using an external standard (Na/SSZ-13 with known Al concentration). Note that Al contents are ~7% lower in Cu/SSZ-13 samples due to minor Al loss in ion-exchange. However, NMR Al content analysis using Cu/SSZ-13 samples is unreliable due to the presence of paramagnetic Cu^{2+} ions. [b)] Determined with ICP. [c)] Assuming ~7% Al loss during ion exchange.

Figure 2 presents standard NH_3-SCR ($4NO + 4NH_3 + O_2 = 4N_2 + 6H_2O$) light-off curves for the three fresh Cu/SSZ-13 catalysts at a GHSV of ~200,000 h^{-1}. It is immediately clear that the three catalysts have essentially identical performance, where excellent NO_x reduction efficiency is achieved within a broad temperature window of 200-450 °C. Note that NO conversions are rather similar under differential conditions (100 and 120 °C, NO conversions ≤15%). This suggests that intra-crystalline mass transfer limitation essentially does not exist under these conditions. Otherwise Cu/SSZ-13 A, which has an average particle size of ~1.3 μm, should display inferior performance as compared to the other two catalysts with considerably smaller primary particle sizes. Between ~140 to ~200 °C, NO conversions on Cu/SSZ-13 A are also only slightly lower than the other two catalysts. To further investigate the hydrothermal stability, samples underwent a severe hydrothermal aging procedure. By essentially steaming

the sample at high temperatures, realistic conditions found in catalytic converters of diesel engines can be simulated [3].

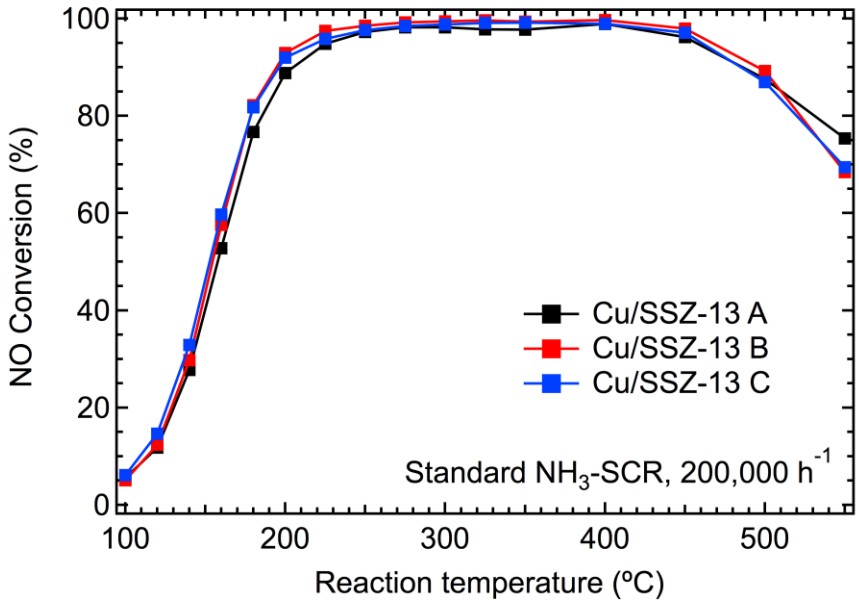

Figure 2. Standard NH_3-SCR light-off curves for the fresh Cu/SSZ-13 samples. All materials exhibit similar performances.

Light-off curves of the hydrothermally aged (16h at 800°C in 10% H_2O) samples are presented in Figure 3 measured under identical conditions. Strikingly, the severe high temperature steaming treatment did not result in a significant reduction in catalytic capability of the small particles, but rather the three catalyst series exhibited similar catalytic performance. Importantly, this is the first time that Cu/SSZ-13 catalysts with primary particle sizes of less than 0.5 µm are demonstrated to be as hydrothermally stable as catalysts with much larger primary particle sizes. Although there is no discernible advantage in the catalytic activity observed for these powder samples, in realistic applications where the Cu/SSZ-13 catalysts are wash-coated, a smaller particle size may still provide considerable advantages. Notably, improved mass and heat transfer due to thinned washcoat layers could be realized for these modified catalysts. This is especially the case for the SCR-DPF concept that has been considered for some time. In this case, the SCR catalyst layer is coated on a diesel particulate filter (DPF) where mass/heat transfer becomes more critical than in a stand-alone SCR catalyst system. Moreover, for thinner SCR catalyst

coatings, it is anticipated that transitioning from the cold-start to normal operation will require shorter times, further facilitating low-temperature NO_x conversion efficiencies.

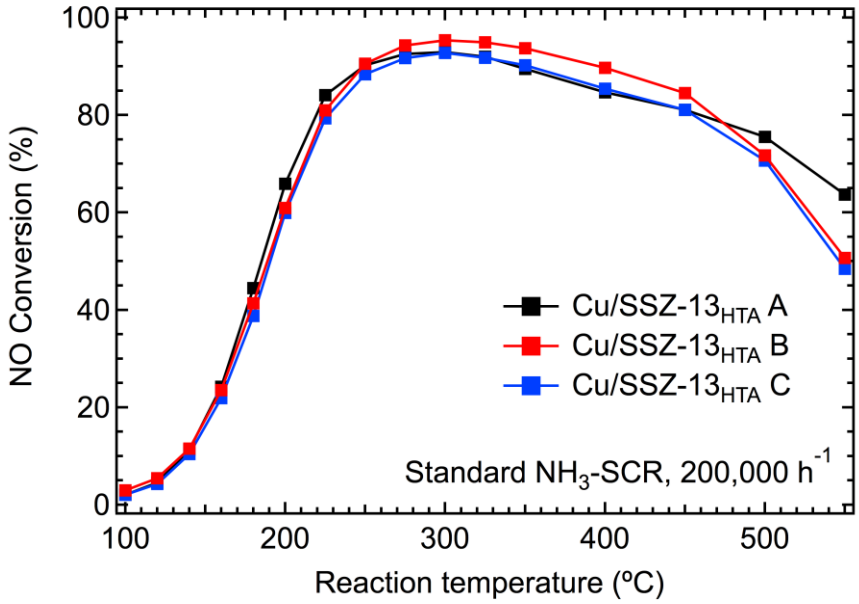

Figure 3. Standard NH_3-SCR light-off curves for the Cu/SSZ-13_{HTA} samples.

3.3 Characterization of hydrothermally aged catalysts

Having established that sub-micron Cu/SSZ-13 performs equally well in SCR reactions as large particles, even after having been exposed to a severe steaming procedure, an investigation was undertaken to gain understanding of this phenomenon. For this purpose both the Cu/SSZ-13 and Na/SSZ-13 forms were treated under hydrothermal conditions. Metal cations typically show positive effects towards zeolite hydrothermal stability: an increased hydrothermal stability was observed for La exchanged zeolite Y, as well as for Cu/SSZ-13 exchanged with different co-cations [13, 34]. However, the types of cations present in the material influence hydrothermal stability differently. For this reason, the severity of the hydrothermal treatment was varied between the Na and Cu forms. The Cu/SSZ-13 materials underwent a more severe hydrothermal aging treatment (16h at 800 °C), compared to the Cu free form Na/SSZ-13, which was aged only at 700 °C for 3h. As a result, the observed macroscopic changes were marginal in both cases. Characterization with X-ray diffraction and nitrogen physisorption for the smallest particles

(Method C) shows no significant changes in the materials properties due to hydrothermal aging (Figure 4). Both Cu/SSZ-13 and Na/SSZ-13 forms exhibit a small loss in micropore volume and a concurrent gain in mesopores as an effect of the steaming procedure (Table S2). At the same time the long-range order as determined by XRD is not diminished, in agreement with previous observations [35]. Moreover, the crystallite size of the synthesized C materials does not change significantly after aging as seen in the Supporting Information (Table S1). The same trends can be observed for the other two synthesis methods (Figures S2 and S4). Thus, no clear structural distinction based on particle size can be made.

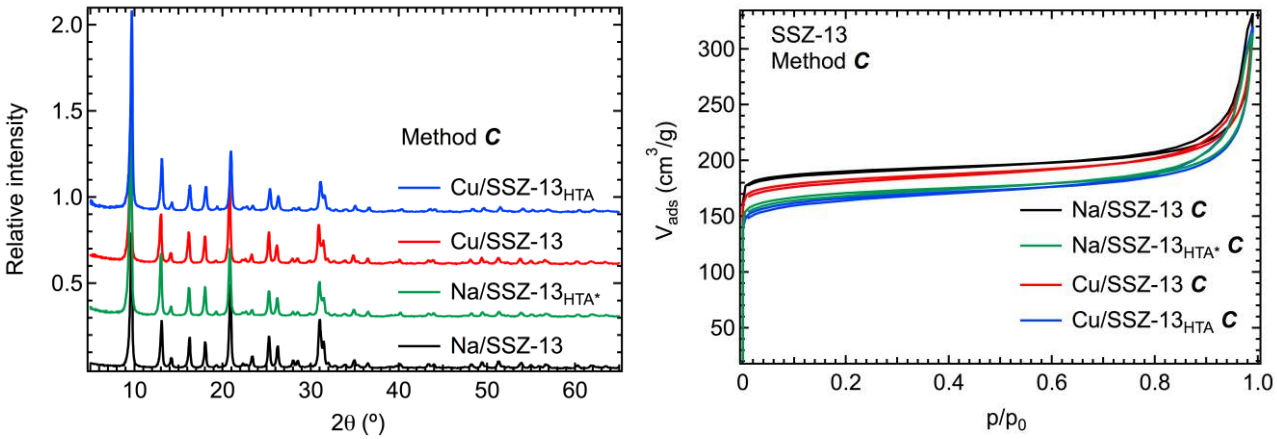

Figure 4. XRD and N_2 physisorption showing the impact of hydrothermally aging on the long range order and porosity of Na and Cu/SSZ-13.

In contrast to XRD, ^{27}Al MAS NMR is substantially more sensitive to changes in the local Al environment. One possible complication is that second order quadrupolar interactions, depending on the nature of the Al nucleus, can result in line broadening of signals beyond detection, i.e., the so-called 'invisible' Al. Using high magnetic fields and low tip angles as was done in this contribution, this effect can be minimized [36, 37]. However, certain highly distorted extra-framework Al species, generated during extensive and severe steaming, may still be invisible even with high magnetic fields [37-39]. The spectra for the various stages of the method C materials are shown in Figure 5. For fresh Na/SSZ-13, almost all Al is tetrahedrally coordinated and fully incorporated in the framework as indicated by the peak at 58 ppm. Only a small amount of extra-framework octahedral Al at 0 ppm is noticeable. For fresh Cu/SSZ-

13, during the washing procedure as part of the Cu exchange step, almost all extra-framework Al is removed. Therefore, the relative contribution of tetrahedral Al is increased in the Cu/SSZ-13 form. Note that in Cu/SSZ-13 samples, paramagnetic Cu species situated next to tetrahedral Al can also cause signal invisibility [35]. To largely mitigate this effect, all of the Cu/SSZ-13 samples were fully hydrated prior to NMR experiments to decrease Al-Cu interactions. In fully hydrated form, Cu-ions preferentially form outer sphere complexes as $[Cu(H_2O)_6]^{2+}$ and $[Cu(OH)(H_2O)_5]^{+}$ in Chabazite cages, thus decreasing direct interactions with the zeolite framework [4, 40, 41]. This was confirmed by determining Al contents for the Cu/SSZ-13 C samples through elemental analysis, showing that NMR invisible Al due to the presence of paramagnetic Cu^{2+} only accounts for no higher than 10% of the total Al (Supporting Information Table S4).

When undergoing hydrothermal aging, the high temperatures and presence of steam leads to dealumination, caused by hydrolysis of the Si-O-Al bonds [42, 43]. As a result, the tetrahedral ^{27}Al NMR peak intensity is significantly reduced, the peak is broadened due to increased heterogeneity of the Al environment, and the concentration of extra-framework species (0 ppm) is increased. The migration of Al from the framework to extra-framework positions also explains the small loss in micropore volume and resulting increased mesopore volume [20].

In addition, some partially framework bonded Al species are formed, leading to the appearance of a peak at 30 ppm associated with pentahedral Al [13]. These latter Al species are connected to the framework by three bonds or less with the coordination sphere of Al being filled by H_2O molecules. However, the dealumination process removes only a small number of Al atoms, with the majority retaining the coherency of the planes relevant for X-ray diffraction, explaining why the long-range order does not change. The same trends are observed for materials obtained with methods A and B, shown in the Supporting Information (Figure S7). It is worthwhile pointing out once more the varying steaming conditions for the Na and Cu forms. Assuming more severe conditions are chosen for Na/SSZ-13, a higher

degree of dealumination could lead to more distinctive changes in the crystallinity, porosity and the state of framework Al.

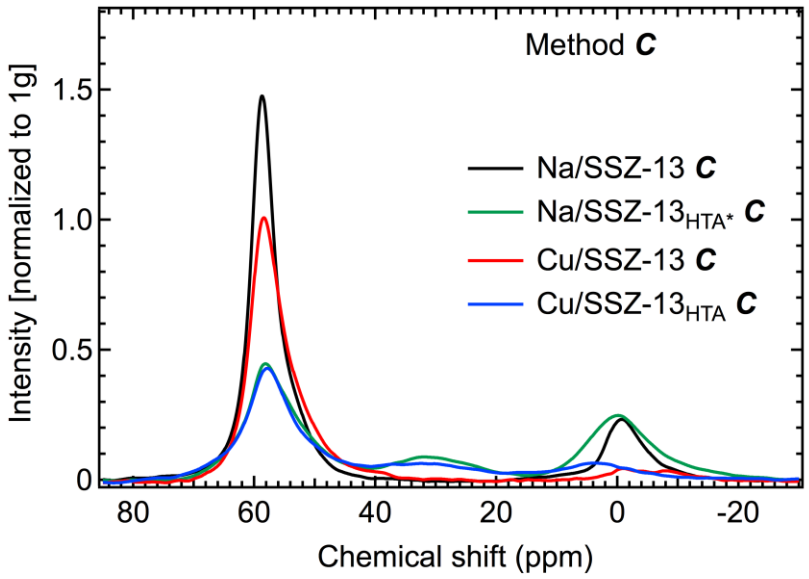

Figure 5. ^{27}Al MAS NMR spectra of fresh and HTA SSZ-13 samples synthesized with method C.

Deconvolution of the spectra shown in Figures 5 (method C) and S7 (methods A and B) allows for the determination of the relative contribution of the respective Al species. The effect of hydrothermal aging on the Al environment in Na/SSZ-13 shown in Figure 6 is first discussed. The extra-framework Al observed in the fresh Na/SSZ-13 form is produced during the template removal step. Note that the as-synthesized materials before template removal contain essentially no octahedral Al (data now shown). At 550°C the organic template molecules are decomposed. This results in the formation of H^+ as charge balancing cations, and the formation of small amounts of octahedral Al. The effect is more pronounced for smaller particles indicating their lower stability. This trend becomes more obvious after hydrothermal aging. Smaller particles obtained with method B and C have significantly less tetrahedral Al left compared to the large particles obtained with method A. For zeolites with other structures, for example BEA [28, 30] and MFI [23], previous studies have shown that smaller particle size leads to lower hydrothermal stability. This study demonstrates that Na/SSZ-13 follows the same trend.

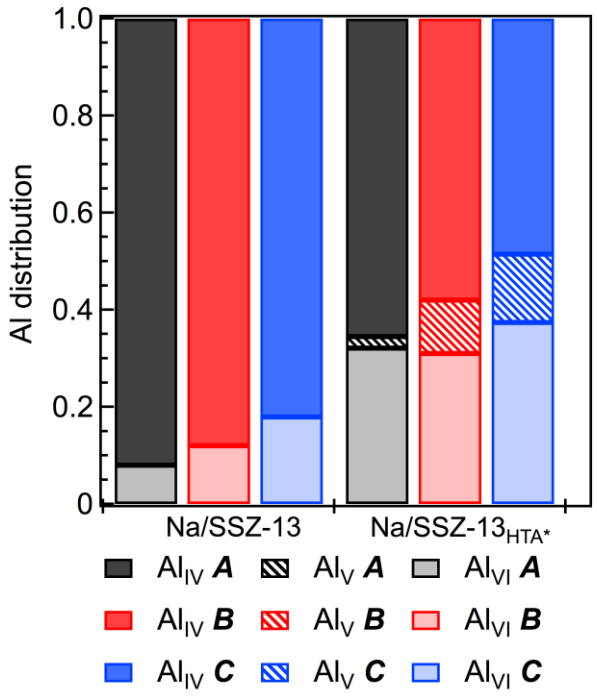

Figure 6. Relative Al contribution of the tetrahedral (Al_{IV}), pentahedral (Al_V) and octahedral (Al_{VI}) species observed with ^{27}Al MAS NMR for fresh and HTA Na/SSZ-13. Color-coding is reported in the legend.

Evaluation of the state of Al in Cu-exchanged, hydrothermally aged SSZ-13 is complicated by line broadening due both to paramagnetic Cu ions and highly distorted Al. Thus, the apparent loss in Al (Supporting Information, Tables S3 and S4) is as high as 40% for all three samples. The residual Al observed with ^{27}Al MAS NMR, however, presents interesting and noteworthy Al distributions, as shown in Figure 7. Specifically, despite the fact that SSZ-13 C displays poorer hydrothermal stability in the Na-form as seen in Figure 6, Cu/SSZ-13 C is capable of retaining more tetrahedral framework Al after hydrothermal aging.

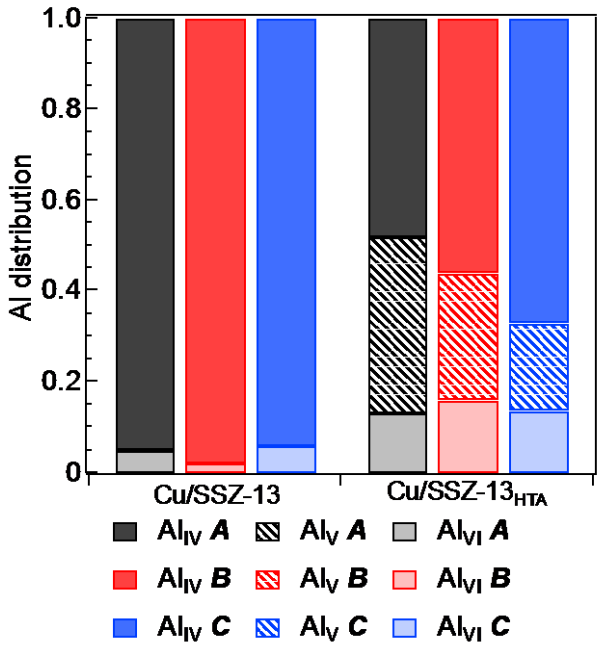

Figure 7. Relative Al contribution of the tetrahedral (Al_{IV}), pentahedral (Al_V) and octahedral (Al_{VI}) species observed with ^{27}Al MAS NMR for fresh and HTA Cu/SSZ-13. Color-coding is reported in the legend.

To better understand this phenomenon, EPR was used to quantify isolated Cu^{2+} ions in Cu/SSZ-13 samples, and the spectra are shown in Figure 8. In order to avoid signal loss due to Cu-Cu dipolar interactions, spectra were recorded at 125 K to freeze Cu-ion mobility. The spectra were double integrated and quantified using standard Cu(II)-imidazole solutions. Also displayed in Figure 8 are molar ratios between EPR active Cu and Al of these samples, where the respective Al concentrations were obtained with NMR and corrected for invisible Al. Details on the calculation of these ratios are displayed in Supporting Information Table S5.

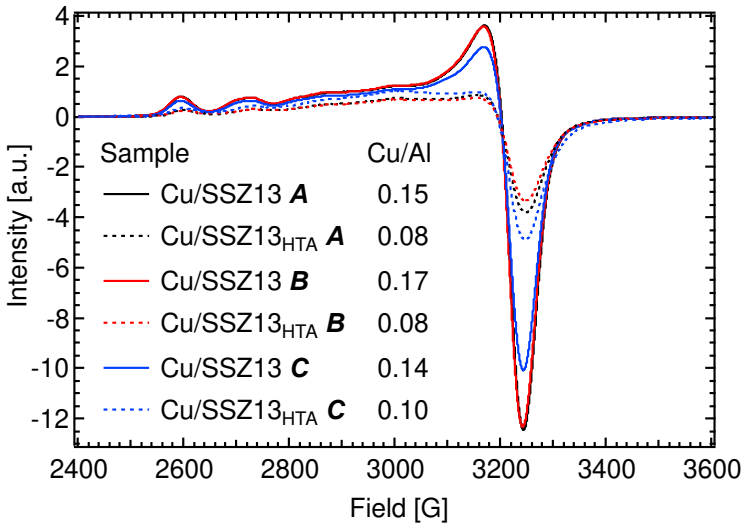

Figure 8. EPR spectra of hydrated Cu/SSZ-13 samples. EPR active Cu^{2+} amounts are reported in molar Cu/Al ratios in the legend. The respective Al concentrations were corrected for the invisible Al, assuming an equal extent irrespective of synthesis method (see Tables S4 and S5). Color-coding is also reported in the legend.

Note that in fresh Cu/SSZ-13 A and B samples, within experimental error, total Cu contents measured with ICP (Table 2) are equal to isolated Cu-ions quantified via EPR (Table S5) demonstrating that essentially all of the Cu in these two samples is isolated. However, fresh Cu/SSZ-13 C contains ~0.3 wt% EPR silent Cu species. This may be correlated with the substantially higher mesopore volume of SSZ-13 C (Table 1) such that during ion exchange, some copper is trapped (instead of ion-exchanged) into the mesopores and subsequently converted to EPR silent CuO_x during calcination. This small portion of Cu does not appear to play a role in affecting SCR reactions (Figures 2, 3). In HTA samples, EPR silent portions of Cu can also be assigned to clustered CuO_x species, which form during hydrothermal aging via migration and agglomeration of the less stable isolated Cu-ions. For the two different isolated Cu-ions in Cu/SSZ-13, i.e., Cu^{2+} ions that are associated with paired framework Al sites, and $[Cu(OH)]^+$ ions that are associated with one framework Al, there has been ample evidence from recent literature to suggest that the $[Cu(OH)]^+$ ions, since these interact more weakly with the CHA framework, are the ones that agglomerate to CuO_x clusters. In contrast, Cu^{2+} ions stabilized by paired framework Al sites survive harsh hydrothermal aging [4-9]. Note that differences in Al and Cu contents among the three

fresh Cu/SSZ-13 samples are never higher than 10%. Interestingly, however, Cu/SSZ-13_{HTA} C contains substantially more EPR active, isolated Cu^{2+} species (up to 30%) than the other two HTA samples. In this regard, the NMR results displayed in Figure 7 are fully consistent with the EPR quantifications of isolated Cu^{2+} sites in HTA samples. Specifically, Cu^{2+} ions appear to have a higher probability in residing in energetically favorable extra-framework sites (i.e., windows of 6MR with Al pairs) in Cu/SSZ-13 C during hydrothermal aging, resulting in better protection of both tetrahedral Al and isolated Cu^{2+} ions. Results shown in Figures 7 and 8 indicate then that SSZ-13 synthesis method C used in this study allows higher paired Al concentrations as compared to the other two methods, even though total Al contents are very similar. Recently, Di Iorio and Gounder demonstrated the feasibility for favoring Al-pair formation in the SSZ-13 framework by controlling interactions between organic and inorganic structure directing agents [44]. From the present study, it is further inferred that other changes to the gel composition, e.g., doubling the Na:Al ratio and increasing the aging time, also have effects on the inherent distribution of Al framework sites.

To summarize, small Na/SSZ-13 particles behave as expected, presenting a poorer hydrothermal stability than the larger counterparts obtained with Method A. This assessment is based on ^{27}Al MAS NMR. The same situation is not found for Cu/SSZ-13. Moreover, after hydrothermal aging, higher EPR active Cu (isolated Cu^{2+}) is even found in Cu/SSZ-13_{HTA} C, accompanied with higher tetrahedral Al in this sample. As has been shown previously, during hydrothermal aging, Cu^{2+} ions balanced by framework Al pairs maintain high stability. In other words, both Cu-ion agglomeration and dealumination are prevented simultaneously for this structure. On the other hand, $[Cu(OH)]^+$ ions tend to agglomerate to non-paramagnetic CuO_x clusters. As a result, framework Al that charge-balance these ions in fresh samples will experience subsequent dealumination upon $[Cu(OH)]^+$ detachment [7]. However, SSZ-13 is capable of maintaining structural integrity to a certain degree of dealumination. We have shown that the long-range order and porosity of the Cu-exchanged system changes very little due to hydrothermal ag-

ing. Therefore, the present study clearly shows that by incorporating Cu-ions, the particle size dependent framework stability can be circumvented, at least up to a hydrothermal aging temperature of 800 °C, producing stable sub-micron Cu/SSZ-13 catalysts. Detailed analyses from NMR and EPR, on the other hand, indicate that both the states of the Al and Cu in Cu/SSZ-13 are affected by the steaming procedure. This is caused by more subtle differences among the zeolite structures, especially the presence of different degrees of Al-pairing affected by changing the gel composition.

However, such structural changes do not seem to have important influences on the overall catalytic performance in SCR reactions (Figure 3). This can in principle be understood from the complexity of the SCR reaction, i.e., it is influenced by multiple factors including redox of the active Cu centers, residual Brønsted acid site densities, and NH_3 storage capacities [1, 8]. For example, the slightly lower active Cu site concentrations for Cu/SSZ-13_{HTA} A and B may be compensated by the presence of suitable NH_3 storage sites (e.g., extra-framework Al) in close vicinity. To gain a better understanding of NH_3 storage to SCR performance, NH_3-TPD were conducted on fresh and HTA Cu/SSZ-13 A and C catalysts and the results are displayed in Fig. S9. As can be seen, NH_3 storage capacity differences between the two fresh and the two HTA samples are rather minor, consistent with the similar SCR performance of the corresponding samples as displayed in Figs. 2 and 3.

4 CONCLUSION

SSZ-13 zeolite materials with the same Si/Al ratio were synthesized via three different procedures yielding particle sizes ranging between 260 nm and 1.3 μm. A longer aging period leads to significantly reduced particle size. The Na/SSZ-13 materials show the expected hydrothermal stability trends in terms of tetrahedral framework Al, evaluated with ^{27}Al MAS NMR. However, after incorporation of Cu ions, standard SCR reaction testing showed that the performance is independent of particle size, even after severe hydrothermal aging. This unprecedented result is attributed to the extraordinary stability of framework Al – extra-framework Cu ensembles against steaming, independent of the particle size. Vehi-

cular DeNOx technologies are prospective candidates for this promising new result as wash coatings can now be improved by applying layers of smaller particle sizes virtually increasing the concentration of active Cu/SSZ-13 species.

ASSOCIATED CONTENT

AUTHOR INFORMATION

Corresponding Authors

* Miroslaw A. Derewinski: miroslaw.derewinski@pnnl.gov,

Feng Gao: feng.gao@pnnl.gov.

ACKNOWLEDGMENT

The authors would like to thank B. W. Arey and J. J. Ditto for performing electron microscope imaging and M. Neukamm for performing AAS measurements. The authors gratefully acknowledge the US Department of Energy (DOE), Energy Efficiency and Renewable Energy, Vehicle Technologies Office for the support of this work. S. P and M. A. D also acknowledge support by the Materials Synthesis and Simulation Across Scales (MS^3 Initiative) conducted under the Laboratory Directed Research & Development Program at PNNL. The research described in this paper was performed in the Environmental Molecular Sciences Laboratory (EMSL), a national scientific user facility sponsored by the DOE's Office of Biological and Environmental Research and located at Pacific Northwest National Laboratory (PNNL). PNNL is operated for the US DOE by Battelle.

REFERENCES

[1] A.M. Beale, F. Gao, I. Lezcano-Gonzalez, C.H.F. Peden, J. Szanyi, Recent advances in automotive catalysis for NOx emission control by small-pore microporous materials, Chem. Soc. Rev., 44 (2015) 7371-7405.
[2] F. Gao, J. Kwak, J. Szanyi, C.F. Peden, Current Understanding of Cu-Exchanged Chabazite Molecular Sieves for Use as Commercial Diesel Engine DeNOx Catalysts, Top. Catal., 56 (2013) 1441-1459.
[3] S.J. Schmieg, S.H. Oh, C.H. Kim, D.B. Brown, J.H. Lee, C.H.F. Peden, D.H. Kim, Thermal durability of Cu-CHA NH3-SCR catalysts for diesel NOx reduction, Catal. Today, 184 (2012) 252-261.
[4] J.H. Kwak, H.Y. Zhu, J.H. Lee, C.H.F. Peden, J. Szanyi, Two different cationic positions in Cu-SSZ-13?, Chem Commun, 48 (2012) 4758-4760.

[5] F. Giordanino, P.N.R. Vennestrom, L.F. Lundegaard, F.N. Stappen, S. Mossin, P. Beato, S. Bordiga, C. Lamberti, Characterization of Cu-exchanged SSZ-13: a comparative FTIR, UV-Vis, and EPR study with Cu-ZSM-5 and Cu-beta with similar Si/Al and Cu/Al ratios, Dalton T, 42 (2013) 12741-12761.
[6] F. Gao, E.D. Walter, M. Kollar, Y.L. Wang, J. Szanyi, C.H.F. Peden, Understanding ammonia selective catalytic reduction kinetics over Cu/SSZ-13 from motion of the Cu ions, J. Catal., 319 (2014) 1-14.
[7] Y.J. Kim, J.K. Lee, K.M. Min, S.B. Hong, I.S. Nam, B.K. Cho, Hydrothermal stability of CuSSZ13 for reducing NOx by NH3, J Catal, 311 (2014) 447-457.
[8] F. Gao, N.M. Washton, Y.L. Wang, M. Kollár, J. Szanyi, C.H.F. Peden, Effects of Si/Al ratio on Cu/SSZ-13 NH3-SCR catalysts: Implications for the active Cu species and the roles of Brønsted acidity, J Catal, 331 (2015) 25-38.
[9] C.W. Andersen, M. Bremholm, P.N.R. Vennestrøm, A.B. Blichfeld, L.F. Lundegaard, B.B. Iversen, Location of Cu2+ in CHA zeolite investigated by X-ray diffraction using the Rietveld/maximum entropy method, IUCrJ, 1 (2014) 382-386.
[10] C. Paolucci, A.A. Parekh, I. Khurana, J.R. Di Iorio, H. Li, J.D. Albarracin Caballero, A.J. Shih, T. Anggara, W.N. Delgass, J.T. Miller, F.H. Ribeiro, R. Gounder, W.F. Schneider, Catalysis in a Cage: Condition-Dependent Speciation and Dynamics of Exchanged Cu Cations in SSZ-13 Zeolites, J. Am. Chem. Soc., 138 (2016) 6028-6048.
[11] F. Goltl, R.E. Bulo, J. Hafner, P. Sautet, What Makes Copper-Exchanged SSZ-13 Zeolite Efficient at Cleaning Car Exhaust Gases?, J Phys Chem Lett, 4 (2013) 2244-2249.
[12] S.A. Bates, A.A. Verma, C. Paolucci, A.A. Parekh, T. Anggara, A. Yezerets, W.F. Schneider, J.T. Miller, W.N. Delgass, F.H. Ribeiro, Identification of the active Cu site in standard selective catalytic reduction with ammonia on Cu-SSZ-13, J Catal, 312 (2014) 87-97.
[13] F. Gao, Y. Wang, N.M. Washton, M. Kollár, J. Szanyi, C.H.F. Peden, Effects of Alkali and Alkaline Earth Cocations on the Activity and Hydrothermal Stability of Cu/SSZ-13 NH3–SCR Catalysts, ACS Catal., 5 (2015) 6780-6791.
[14] U. Deka, A. Juhin, E.A. Eilertsen, H. Emerich, M.A. Green, S.T. Korhonen, B.M. Weckhuysen, A.M. Beale, Confirmation of Isolated Cu2+ Ions in SSZ-13 Zeolite as Active Sites in NH3-Selective Catalytic Reduction, J. Phys. Chem. C, 116 (2012) 4809-4818.
[15] S. Prodinger, R.S. Vemuri, T. Varga, B.P. McGrail, R.K. Motkuri, M.A. Derewinski, Impact of chabazite SSZ-13 textural properties and chemical composition on CO_2 adsorption applications, New J. Chem., 40 (2016) 4375-4385.
[16] F. Gao, E.D. Walter, E.M. Karp, J.Y. Luo, R.G. Tonkyn, J.H. Kwak, J. Szanyi, C.H.F. Peden, Structure-activity relationships in NH3-SCR over Cu-SSZ-13 as probed by reaction kinetics and EPR studies, J. Catal., 300 (2013) 20-29.
[17] C. Baerlocher, L.B. McCusker, Database of Zeolite Structures.
[18] A.N.C. van laak, R.W. Gosselink, S.L. Sagala, J.D. Meeldijk, P.E. de Jongh, K.P. de Jong, Alkaline treatment on commercially available aluminum rich mordenite, Appl. Catal., A, 382 (2010) 65-72.
[19] Y. Tao, H. Kanoh, L. Abrams, K. Kaneko, Mesopore-Modified Zeolites: Preparation, Characterization, and Applications, Chem. Rev., 106 (2006) 896-910.
[20] J.C. Groen, J.A. Moulijn, J. Pérez-Ramírez, Decoupling mesoporosity formation and acidity modification in ZSM-5 zeolites by sequential desilication–dealumination, Microporous Mesoporous Mater., 87 (2005) 153-161.
[21] C.S. Cundy, P.A. Cox, The hydrothermal synthesis of zeolites: Precursors, intermediates and reaction mechanism, Microporous Mesoporous Mater., 82 (2005) 1-78.
[22] C.S. Cundy, Synthesis of zeolites and zeotypes, in: J. Čejka, H.v. Bekkum (Eds.) Stud. Surf. Sci. Catal., Elsevier2005, pp. 65-90.
[23] E.J.P. Feijen, J.A. Martens, P.A. Jacobs, Hydrothermal Zeolite Synthesis, in: G. Ertl, H. Knözinger, J. Weitkamp (Eds.) Preparation of Solid Catalysts, Wiley-VCH Verlag GmbH2008, pp. 262-284.
[24] E.J.P. Feijen, J.A. Martens, P.A. Jacobs, Zeolites and their Mechanism of Synthesis, in: H.G.K.H.P. J. Weitkamp, W. Hölderich (Eds.) Stud. Surf. Sci. Catal., Elsevier1994, pp. 3-21.
[25] A.W. Burton, K. Ong, T. Rea, I.Y. Chan, On the estimation of average crystallite size of zeolites from the Scherrer equation: A critical evaluation of its application to zeolites with one-dimensional pore systems, Microporous Mesoporous Mater., 117 (2009) 75-90.
[26] L. Ding, Y. Zheng, Z. Zhang, Z. Ring, J. Chen, Effect of agitation on the synthesis of zeolite beta and its synthesis mechanism in absence of alkali cations, Microporous Mesoporous Mater., 94 (2006) 1-8.
[27] M. Derewinski, M. Machowska, Effect of stirring on the selective synthesis of mel or ton zeolites in the presence of 1,8-diaminooctane, in: E. van Steen, I.M. Claeys, L.H. Callanan (Eds.) Stud. Surf. Sci. Catal., Elsevier2004, pp. 349-354.
[28] M. Iwasaki, K. Yamazaki, H. Shinjoh, NOx reduction performance of fresh and aged Fe-zeolites prepared by CVD: Effects of zeolite structure and Si/Al2 ratio, Applied Catalysis B: Environmental, 102 (2011) 302-309.
[29] M.A. Camblor, A. Corma, S. Valencia, Characterization of nanocrystalline zeolite Beta, Microporous Mesoporous Mater., 25 (1998) 59-74.
[30] J. Panpranot, U. Toophorm, P. Praserthdam, Effect of Particle Size on the Hydrothermal Stability and Catalytic Activity of Polycrystalline Beta Zeolite, J. Porous Mater., 12 (2005) 293-299.
[31] H. Xiong, H.N. Pham, A.K. Datye, Hydrothermally stable heterogeneous catalysts for conversion of biorenewables, Green Chemistry, 16 (2014) 4627-4643.
[32] S. Moreno, G. Poncelet, Dealumination of small- and large-port mordenites: A comparative study, Microporous Mater., 12 (1997) 197-222.
[33] C.S. Triantafillidis, N.P. Evmiridis, L. Nalbandian, I.A. Vasalos, Performance of ZSM-5 as a Fluid Catalytic Cracking Catalyst Additive: Effect of the Total Number of Acid Sites and Particle Size, Ind. Eng. Chem. Res., 38 (1999) 916-927.
[34] F. Maugé, P. Gallezot, J.-C. Courcelle, P. Engelhard, J. Grosmangin, Hydrothermal aging of cracking catalysts. II. Effect of steam and sodium on the structure of La-Y zeolites, Zeolites, 6 (1986) 261-266.
[35] J.H. Kwak, D. Tran, S.D. Burton, J. Szanyi, J.H. Lee, C.H.F. Peden, Effects of hydrothermal aging on NH3-SCR reaction over Cu/zeolites, J. Catal., 287 (2012) 203-209.
[36] C.A. Fyfe, J.L. Bretherton, L.Y. Lam, Detection of the 'invisible aluminium' and characterisation of the multiple aluminium environments in zeolite USY by high-field solid-state NMR, Chem. Commun., (2000) 1575-1576.
[37] C.A. Fyfe, J.L. Bretherton, L.Y. Lam, Solid-State NMR Detection, Characterization, and Quantification of the Multiple Aluminum Environments in US-Y Catalysts by 27Al MAS and MQMAS Experiments at Very High Field, J. Am. Chem. Soc., 123 (2001) 5285-5291.
[38] J.A. van Bokhoven, A.L. Roest, D.C. Koningsberger, J.T. Miller, G.H. Nachtegaal, A.P.M. Kentgens, Changes in Structural and Electronic Properties of the Zeolite Framework Induced by Extraframework Al and La in H-USY and La(x)NaY: A 29Si and 27Al MAS NMR and 27Al MQ MAS NMR Study, J. Phys. Chem. B, 104 (2000) 6743-6754.
[39] E. Lippmaa, A. Samoson, M. Magi, High-resolution aluminum-27 NMR of aluminosilicates, J. Am. Chem. Soc., 108 (1986) 1730-1735.
[40] J.S. McEwen, T. Anggara, W.F. Schneider, V.F. Kispersky, J.T. Miller, W.N. Delgass, F.H. Ribeiro, Integrated operando X-ray absorption and DFT characterization of Cu–SSZ-13 exchange sites during the selective catalytic reduction of NOx with NH3, Catal. Today, 184 (2012) 129-144.
[41] J.H. Kwak, T. Varga, C.H.F. Peden, F. Gao, J.C. Hanson, J. Szanyi, Following the movement of Cu ions in a SSZ-13 zeolite during dehydration, reduction and adsorption: A combined in situ TP-XRD, XANES/DRIFTS study, J. Catal., 314 (2014) 83-93.
[42] E. Bourgeat-Lami, P. Massiani, F. Di Renzo, P. Espiau, F. Fajula, T. Des Courières, Study of the state of aluminium in zeolite-β, Applied Catalysis, 72 (1991) 139-152.

[43] J.A. van Bokhoven, D.C. Koningsberger, P. Kunkeler, H. van Bekkum, A.P.M. Kentgens, Stepwise Dealumination of Zeolite Beta at Specific T-Sites Observed with 27Al MAS and 27Al MQ MAS NMR, J. Am. Chem. Soc., 122 (2000) 12842-12847.
[44] J.R. Di Iorio, R. Gounder, Controlling the Isolation and Pairing of Aluminum in Chabazite Zeolites Using Mixtures of Organic and Inorganic Structure-Directing Agents, Chem. Mater., 28 (2016) 2236-2247.

TOC image

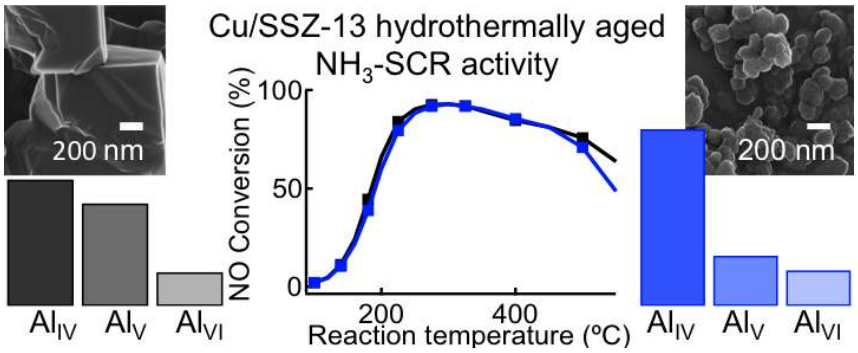
200 nm
Cu/SSZ-13 hydrothermally aged
NH3-SCR activity
NO Conversion (%)
100
50
0
200
400
Reaction temperature (ºC)
AlIV
AlV
AlVI
200 nm
AlIV
AlV
AlVI